

Effect of an external electric field on local magnetic moments in silicene

J. Villarreal[†], F. Escudero[†], J. S. Ardenghi^{†*} and P. Jasen[†]
 IFISUR, Departamento de Física (UNS-CONICET)
 Avenida Alem 1253, Bahía Blanca, Buenos Aires, Argentina

January 5, 2021

Abstract

In this work we analyze the effects of the application of an external electric field in the formation of a local magnetic moment in silicene. By adding an impurity in a top site in the host lattice and computing the real and imaginary part of the self-energy of the impurity energy level, the polarized density of states is used in order to obtain the occupation number of the up and down spin formation in the impurity considering the mean field approximation. Unequal occupation numbers is the precursor of a formation of a local magnetic moment and this depends critically on the Hubbard parameter, the on-site energy of the impurity, the spin-orbit interaction in silicene and the electric field applied. In particular, it is shown that in the absence of electric field, the boundary between the magnetic and non-magnetic phases increases with the spin-orbit interaction with respect to graphene with a top site impurity and shrinks and narrows it when the electric field is turned on. The electric field effect is studied for negative and positive on-site impurity energies generalizing the results obtained in the literature for graphene.

1 Introduction

In solid state physics, two dimensional (2D) systems have become one of the most significant topics, where applications in nanoelectronics and spintronics become possible due to the exotic electronic structures of these 2D materials ([1], [2]). The most well known is graphene, a two dimensional honeycomb lattice of carbon atoms [3], but other new developed 2D materials have arisen, such as molybdenum disulfide (MoS₂) [4], silicene [5], germanene ([6] and [7]), phosphorene [8], transition-metal dichalcogenides and hexagonal boron nitride [9] and two-dimensional SiC monolayers [10], that are similar to graphene but with different atoms at each lattice site but with a buckled structure. Due to the intrinsic low electron and phonon densities, 2D materials are ideal platforms to host single atoms with magnetic moments pointing out-of-plane with potential applications in current information nanotechnology. Among these materials, silicene is particularly interesting thanks to its compatibility with the current Si-based electronic technology. In 2010, the synthesis of silicene nanoribbons on the anisotropic Ag(110) surface and on Ag(111) was reported ([11], [12]), showing that silicene has a larger in-plane lattice constant, with two interpenetrating sublattices displaced vertically with respect to each other due to the sp^3 hybridization. In turn, the buckling of silicene can be influenced by the interaction with a ZrB₂ substrate which allows to tune the band gap at the K or K' points in the Brillouin zone [13]. By applying the tight binding model on silicene it is possible to compute the long wavelength approximation in order to obtain an effective Dirac-like Hamiltonian ([1] and [14] and [15]), and around the Fermi energy, the charge carriers behaves as massive Dirac fermions in the π bands moving with a Fermi velocity $v_F = 5.5 \times 10^5$ m/s ([16] [17]). The layer separation between the sublattices in silicene

*email: jsardenghi@gmail.com, fax number: +54-291-4595142

due to its buckled structure, is suitable for application of external fields in order to open a bandgap that introduces diagonal terms in the Hamiltonian written in the A and B sublattices ([18], [19], [5]). The spin-orbit interaction (SOI) in silicene is about 3.9 meV, larger than that of graphene, where is of the order of 10^{-3} meV ([20], [21]). The large SOI allows the quantum spin Hall effect to be observed which implies that silicene becomes a topological insulator ([22], [23]). The interplay between the SOI and external electric field can induce transitions from topological to band insulators allowing valley effects in the conductivity ([18], [24]).

When impurity atoms are deposited on graphene or silicene they can be adsorbed on different adsorption sites, where the most usual is the six-fold hollow site of the honeycomb lattice, on top of a carbon or silicon atom or the two-fold bridge site of neighboring atoms of the host lattice ([25], [26], [27], [28] and [29]). In turn, adatoms bonded to the surface of graphene can lead to a quasi-localized state where the wave function includes contributions from the orbitals of neighboring carbon atoms ([30], [31]).

In particular, when the impurity atoms are magnetic, the strong coupling between the localized magnetic state of the adatom and the band of the 2D host lattice allows non-trivial effects in the static properties of the system, such as the Kondo effect, where the local density of states show a resonance at the Fermi level [32] due to the screening of the magnetic moment of the adatom by the surrounding itinerant electrons. In graphene, the Kondo effect has been reported with Co adatoms spectroscopy [33], but not much is known about the spectral features or Kondo effect in other 2D materials such as silicene. In silicene, the effect of different magnetic adatoms has been studied by using density functional theory ([34], [35], [36] and [37]), showing that silicene is able to form strong bonds with transition metals due to its buckled form and that its properties can be tailored to design batteries [38].

In turn, it has been shown that the magnetic properties of 2D materials are very sensitive to the SOI and the application of external electric and magnetic fields ([39], [40]). These properties can be altered when impurity atoms are introduced in the material because it induces the formation of local magnetic moments. Thus, while there are several numerical studies about transition metal adsorption in silicene and other two-dimensional materials, not much is known about the dependence of the localized magnetic moment on the applied external electric field. The tight-binding method combined with the mean-field approximation [41] allows studying the dependence of the local magnetism with the strong correlation effects of the inner shell electrons, parametrized by the on-site Hubbard contribution and the hybridization of the impurity orbital with the host lattice. By computing the spin-polarized density of states with Green function methods it is possible to obtain the occupation number of each spin in the adatom ([26], [42]). Moreover, the effect of the SOI and an external electric field can tailor the magnetic properties due to the interplay of the level broadening and the sublattice asymmetry that induces a bandgap.

Motivated by this, in this paper we study the magnetic regime of the impurity atom as a function of the Fermi level, the Hubbard parameter, the SOI and an external electric field and we compare it with those obtained in graphene. In particular we will consider impurity atoms adsorbed in a top site in silicene with on-site energy below and above the Dirac point. Based on these results it is possible to study the formation of localized magnetic states in the impurities and their dependence with the external electric field and the asymmetric hybridization with the host lattice. In turn, the boundary between different magnetic phases can be approximated in terms of the Fermi energy and the Hubbard parameter. In this sense, while there are several works with *ab-initio* calculations with different transition metals, not much is known about the magnetic features of silicene with respect to the different parameters in the Hamiltonian. This work will be organized as follows: In section II, the tight-binding model with adatoms is introduced and the Anderson model in the mean-field approximation is applied to silicene. In section III, the results are shown, and a discussion is given and the principal findings of this paper are highlighted in the conclusion.

2 Theoretical model

The tight-binding Hamiltonian of silicene with spin-orbit coupling and a perpendicular electric field reads (see [5])

$$H_0 = -t \sum_{\langle i,j \rangle, s} a_{i,s}^\dagger b_{j,s} + h.c. + \frac{i\lambda_{SO}}{3\sqrt{3}} \sum_{\langle\langle i,j \rangle\rangle, s} s(\nu_{ij} a_{i,s}^\dagger a_{j,s} + \nu_{ij} b_{i,s}^\dagger b_{j,s}) - elE_z \sum_{i,s} \mu_i (a_{i,s}^\dagger a_{j,s} + b_{i,s}^\dagger b_{j,s}) \quad (1)$$

where $a_{i,s}^\dagger (a_{j,s})$ are the creation (annihilation) operators in the sublattice A and $b_{i,s}^\dagger (b_{j,s})$ are the creation (annihilation) operators in the sublattice B of silicene in the site i with spin $s = \pm 1$. The first term of the last equation is the kinetic energy which is $t_{gr} = 2.7\text{eV}$ for graphene and $t_{sil} = 1.6\text{eV}$ for silicene. The second term represents the effective spin-orbit coupling with $\lambda_{SO} = 3.9\text{ meV}$ for silicene (see [5]) and $\nu_{ij} = (\mathbf{d}_i \times \mathbf{d}_j) / |\mathbf{d}_i \times \mathbf{d}_j| = \pm 1$, depending on the orientation of the two nearest neighbor bonds \mathbf{d}_i and \mathbf{d}_j that connect the next nearest neighbors \mathbf{d}_{ij} (see [43] and [44]). The last term is the staggered sublattice potential with $\mu_i = +1(-1)$ for the A and B sublattice sites, where the buckling for silicene is $l_{sil} = 0.23\text{\AA}$ [5] and e is the electron charge. We are not considering the Rashba spin-orbit coupling because it has a negligible effect on the dispersion relation, being comparable to λ_{so} only at the near edge of the Brillouin zone [45].

The basis vectors for the hexagonal Bravais lattice can be written as $\mathbf{R}_{n,m} = n\mathbf{a}_1 + m\mathbf{a}_2$ where n, m are integer numbers, $\mathbf{a}_1 = \frac{a}{2}(3, \sqrt{3}, 0)$ and $\mathbf{a}_2 = \frac{a}{2}(3, -\sqrt{3}, 0)$ are the primitive basis vectors (see red hexagonal in figure 1). Considering the Fourier transform of the creation and annihilation operators $a_{j,s} = \frac{1}{\sqrt{N}} \sum_{\mathbf{k}} e^{-i\mathbf{k}\mathbf{R}_j} a_{\mathbf{k},\sigma}$ and $b_{j,s} = \frac{1}{\sqrt{N}} \sum_{\mathbf{k}} e^{-i\mathbf{k}\mathbf{R}_j} b_{\mathbf{k},\sigma}$ where $j = (n, m)$, the Hamiltonian H_0 becomes

$$H_0 = -t \sum_{\mathbf{k}, s} \phi_{\mathbf{k}} a_{\mathbf{k},s}^\dagger b_{\mathbf{k},s} + h.c. + \sum_{\mathbf{k}, s} \left(\frac{i\lambda_{SO}}{3\sqrt{3}} s \xi_{\mathbf{k}} - elE_z \right) (a_{\mathbf{k},s}^\dagger a_{\mathbf{k},s} - b_{\mathbf{k},s}^\dagger b_{\mathbf{k},s}) \quad (2)$$

where $\phi_{\mathbf{k}} = \sum_{i=1}^3 e^{i\mathbf{k}\cdot\delta_i} e^{ik_z(h_A - h_B)} = \sum_{i=1}^3 e^{i\mathbf{k}\cdot\delta_i} e^{ik_z 2l}$ and $\xi_{\mathbf{k}} = \sum_{i=1}^6 e^{i\mathbf{k}\cdot\mathbf{n}_i}$, where $\delta_1 = \frac{a}{2}(1, \sqrt{3}, 0)$, $\delta_2 = \frac{a}{2}(1, -\sqrt{3}, 0)$ and $\delta_3 = a(1, 0, 0)$ are the next nearest neighbor vectors, whereas $\mathbf{n}_1 = -\mathbf{n}_2 = \mathbf{a}_1$, $\mathbf{n}_3 = -\mathbf{n}_4 = \mathbf{a}_2$ and $\mathbf{n}_5 = -\mathbf{n}_6 = \mathbf{a}_1 - \mathbf{a}_2$ are the six next-nearest neighbor hopping sites (see figure 1) that connect identical sublattice sites. Notice that $\phi_{\mathbf{k}}$ contains the contribution of the buckled structure in the z direction given by the factor $e^{ik_z(h_A - h_B)}$, where $h_{A/B}$ are the sublattice A and B heights with respect to the middle of the buckling, which obey $h_A - h_B = 2l$ (see figure 1) and k_z is the wave-vector in the z direction, in contrast to $\xi_{\mathbf{k}}$ that does not depend on l because next-nearest neighbors belong to the same sublattice, Ab-initio calculations have shown that there are two most stable sites in which transition metals can be adsorbed in two-dimensional systems: the center of the hexagon and the bridge between two atoms [34]. In silicene, the adsorbed atoms preserve the buckled structure, although small distortions in the geometry near the adsorbed atoms appear changing the local buckling. This warping of the silicene sheet can alter the distance between the adatom and the neighboring silicon atoms. The transition metal atoms most likely hybridize at the hollow site via s , d or f orbitals [46]. For simplicity we will consider an impurity atom adsorbed in the top site (A sublattice), with a height h with respect to the A silicon (see figure 1) and neglect small distortions of the buckled structure. In turn, the orbital symmetry that sits on top is not particularly important and we will consider only an s orbital. Considering that the adatom is fixed in a position \mathbf{R}_0 and hybridizes with the sublattice A with strength V , the hybridization Hamiltonian can be written as

$$H_V = V \sum_s a_{0,s}^\dagger (\delta'_{0A}) f_s + h.c. \quad (3)$$

where $\delta'_{0A} = (h - l)e_z$ where $h - l$ is the distance between the impurity and the A silicon atom and f_s annihilates an electron in the magnetic impurity. In the momentum representation, this last

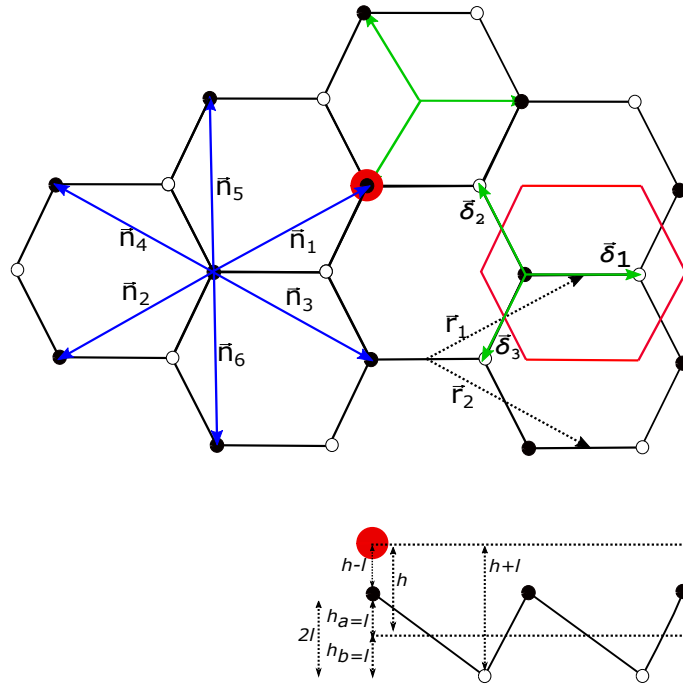


Figure 1: Up. Silicene honeycomb lattice (black and white dots are silicon atoms). Green arrows represent nearest neighbors and blue arrows represent next-nearest neighbors, \mathbf{r}_1 and \mathbf{r}_2 are the lattice vectors and the red hexagon is a particular Bravais lattice. Red point represent impurity adsorbed on a top site. Down: Side view of silicene with the adsorbed impurity where $l(h)$ is the distance of each sublattice(impurity) with respect the middle of the buckling.

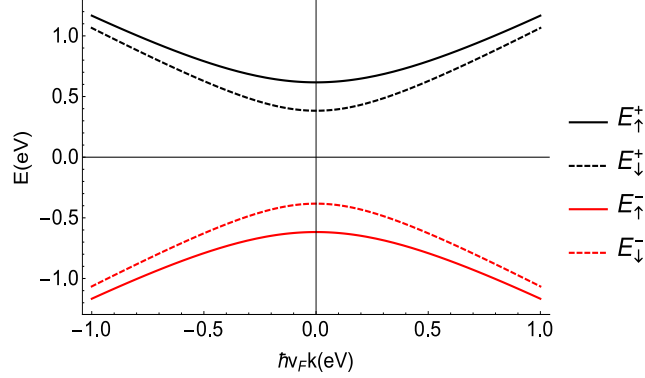


Figure 2: Dispersion relation in the long-wavelength approximation for silicene for each spin, where $elE_z = 0.5$ eV and $\lambda = 0.039$ eV, (\pm) for conduction (valence) band.

Hamiltonian can be written as

$$H_V = \sum_{\mathbf{k},s} V e^{ik_z(h-l)} a_{\mathbf{k},s}^\dagger f_s + h.c. \quad (4)$$

Finally, in order to consider the interaction between electrons in the impurity, we can add the Hamiltonian

$$H_F = [\epsilon_0 - (1+r)elE_z] \sum_s n_s + U n_\uparrow n_\downarrow \quad (5)$$

where ϵ_0 contains the single electron energy at the impurity atom, $r = l_I/l$, where l_I is the distance between the magnetic impurity and the A sublattice, $n_s = f_s^\dagger f_s$ is the occupation number operator for the impurity with spin s and elE_z is the staggered potential. For simplicity we are not considering the redistribution of charges due to the electric field [47]. The Hubbard parameter U characterizes the strength of the electron correlations in the inner shell states of the impurity. By adopting the mean field approximation ([41]), the Hamiltonian H_F can be decomposed in a constant term and the electronic correlations at the impurities $U n_\uparrow n_\downarrow \sim U \sum_s \langle n_s \rangle n_s - U \langle n_\uparrow \rangle \langle n_\downarrow \rangle$, such that the Hamiltonian of the impurity can be rewritten as $H_F = \sum_s \epsilon_s n_s$, where $\epsilon_s = \epsilon + U \langle n_{-s} \rangle$, and $\epsilon = \epsilon_0 - (1+r)elE_z$ is the effective on-site energy of the impurity and the remaining term $-U \langle n_\uparrow \rangle \langle n_\downarrow \rangle$ can be dropped. Then, by considering eq.(2), eq.(4) and eq.(5) the Hamiltonian in compact form can be written in matrix form in the basis $(\Psi_{A,\uparrow}, \Psi_{B,\uparrow}, \Psi_{A,\downarrow}, \Psi_{B,\downarrow}, \Psi_{I,\uparrow}, \Psi_{I,\downarrow})$ as

$$H = \sum_{\mathbf{k},s} \begin{pmatrix} a_{\mathbf{k},\uparrow}^\dagger & b_{\mathbf{k},\uparrow}^\dagger & a_{\mathbf{k},\downarrow}^\dagger & b_{\mathbf{k},\downarrow}^\dagger & f_\uparrow^\dagger & f_\downarrow^\dagger \end{pmatrix} \times \quad (6)$$

$$\begin{pmatrix} -\Delta_{\mathbf{k}\uparrow} & \phi_{\mathbf{k}}^* & 0 & 0 & V & 0 \\ \phi_{\mathbf{k}} & \Delta_{\mathbf{k}\uparrow} & 0 & 0 & 0 & 0 \\ 0 & 0 & -\Delta_{\mathbf{k}\downarrow} & \phi_{\mathbf{k}}^* & 0 & V \\ 0 & 0 & \phi_{\mathbf{k}} & \Delta_{\mathbf{k}\downarrow} & 0 & 0 \\ V & 0 & 0 & 0 & \epsilon + U \langle n_\downarrow \rangle & 0 \\ 0 & 0 & V & 0 & 0 & \epsilon + U \langle n_\uparrow \rangle \end{pmatrix} \begin{pmatrix} a_{\mathbf{k},\uparrow} \\ b_{\mathbf{k},\uparrow} \\ a_{\mathbf{k},\downarrow} \\ b_{\mathbf{k},\downarrow} \\ f_\uparrow \\ f_\downarrow \end{pmatrix}$$

where $\Delta_{\mathbf{k}s} = \frac{i\lambda s Q}{3\sqrt{3}} s \xi_{\mathbf{k}} - elE_z$ and $\phi_{\mathbf{k}} = t \sum_{i=1}^3 e^{i\mathbf{k}\cdot\delta_i}$. The local density of states $\rho_s(\omega)$ at the impurity can be obtained as $\rho_s(\omega) = -\frac{1}{\pi} \Im g_s(\omega)$, where $g_s = \langle f_s | G | f_s \rangle$ is the Green function element for each spin

s at the impurity level. By solving $G = (zI - H)^{-1}$ in the $a_{\mathbf{k},s}$, $b_{\mathbf{k},s}$ and f_s basis, a coupled algebraic system is obtained, where the matrix element $g_s = \langle f_s | G | f_s \rangle$ reads

$$g_s = \frac{1}{z - \epsilon_s - \Sigma_s} \quad (7)$$

where $z = \omega + i0^+$ and Σ_s is the self-energy

$$\Sigma_s = \sum_{\mathbf{k}, \alpha = \pm 1} \frac{\sigma_{\mathbf{k}\alpha s}}{z - \alpha \epsilon_{\mathbf{k}s}} \quad (8)$$

where

$$\sigma_{\mathbf{k}\alpha s} = \frac{V^2}{2} \left(1 + \frac{\alpha \Delta_s}{\epsilon_{\mathbf{k}s}} \right) \quad (9)$$

where $\Delta_s = e l E_z - s \lambda_{so}$ and where

$$\epsilon_{\mathbf{k}s} = \sqrt{(E_z - s \lambda_{so})^2 + \hbar v_F^2 k^2} \quad (10)$$

is the low energy dispersion relation of electrons in silicene with spin-orbit coupling, obtained expanding the numerator and denominator of $\xi_{\mathbf{k}}$ and $\phi_{\mathbf{k}}$ around the K point in the Brillouin zone. From the last equation we can note that there are four bands for $\alpha, s = \pm 1$ describing electrons ($\alpha = 1$) or holes ($\alpha = -1$) with spin s . The bandgap $2|\Delta_s| \sim 1.5$ meV for $e l E_z 0.5$ eV turns silicene into a semiconductor, in contrast to graphene, and the dependence of the gap with the spin is explicit (see figure 2). By computing the imaginary part of the local Green function g_s at the impurity, the local spin density of states can be obtained as

$$\rho_s(\omega) = -\frac{1}{\pi} \Im g_s = \frac{\Im \Sigma_s}{(Z_s^{-1}(\omega)\omega - \epsilon_s)^2 + \Im^2 \Sigma_s} \quad (11)$$

where $Z_s^{-1}(\epsilon) = 1 - \frac{\Re \Sigma_s}{\omega}$ is the quasiparticle residue and $\Re \Sigma_s$ ($\Im \Sigma_s$) is the real (imaginary) part of the self-energy which can be written as

$$\Re \Sigma_s = \sum_{k, \alpha = \pm 1} \frac{\sigma_{\mathbf{k}\alpha s}}{\omega - \alpha \epsilon_{\mathbf{k}s}} \quad \Im \Sigma_s = \pi \sum_{k, \alpha = \pm 1} \sigma_{\mathbf{k}\alpha s} \delta(\omega - \alpha \epsilon_{\mathbf{k}s}) \quad (12)$$

Computing the integral of eq.(12), the real and imaginary part of the self energy reads

$$\begin{aligned} \Re \Sigma_s &= \frac{V^2}{D^2} (\Delta_s - \omega) \ln \left(\left| \frac{\omega^2 - \Delta_s^2 - D^2}{\omega^2 - \Delta_s^2} \right| \right) \\ \Im \Sigma_s &= \frac{\pi V^2}{D^2} (\Delta_s - \omega) [\theta(|\Delta_s| - \omega) - \theta(|\Delta_s| + \omega)] \theta(D - |\omega|) \end{aligned} \quad (13)$$

where $D \sim 7$ eV is the bandwidth, and where $\theta(\sqrt{\Delta_s^2 + D^2} - \omega)$ and $\theta(\sqrt{\Delta_s^2 + D^2} + \omega)$ have been disregarded from the last equation because they only introduce changes for $|\omega| > D$. The last results are a generalization of [48] for the top site with $\Delta_s = 0$ in graphene. In figure (3) the real and imaginary part of the polarized self-energy are shown for different values of the staggered potential. In contrast to graphene, $\Im \Sigma_s$ and $\Re \Sigma_s$ are not symmetric with respect to the Dirac point as it happens for adatoms on top carbon atoms [49]. This is due to the presence of Δ_s which causes an asymmetry that increases with the external electric field applied (see figure 3). Eq.(13) indicates that the level broadening scales as $|\Delta_s - \omega|$ and is identical to zero for $|\omega| < |\Delta_s|$. The real part of the self-energy shifts the assumed unperturbed energy ω and, in contrast to graphene, it is not identical to zero at the Dirac point (see figure 4). The particle-hole symmetry breaking occurs in the whole spectrum in contrast with s orbitals for hollow site adatoms in graphene, where the asymmetry is only evident in the high energy sector ([49], [50]).

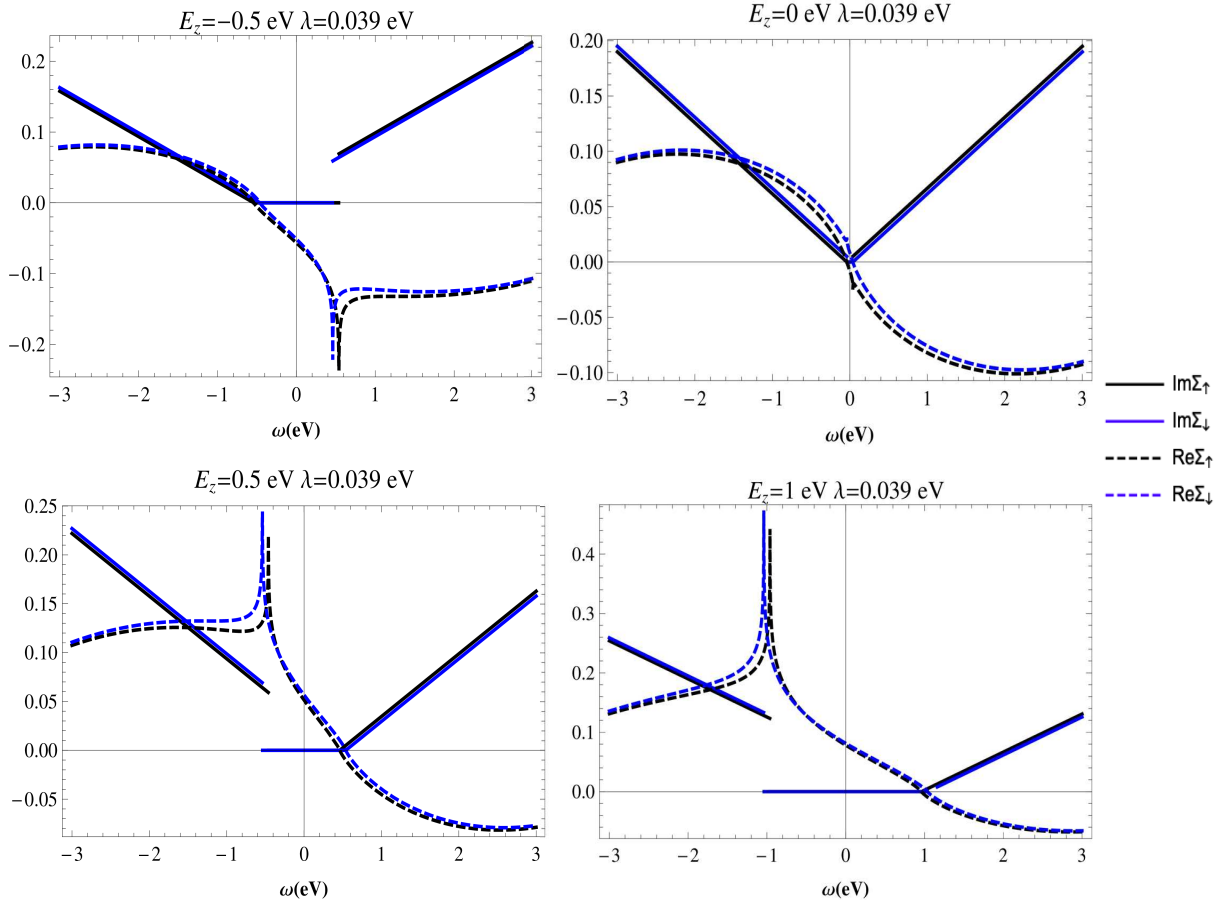


Figure 3: Real $\Re\Sigma_s$ and imaginary $\Im\Sigma_s$ part of the self-energy for different staggered potential values and where we have used that $D = 7\text{eV}$, $V = 0.9\text{ eV}$, $\epsilon_0 = 0.2\text{ eV}$, $U = 0$ and $\lambda = 0.039\text{ eV}$ and $t = 1.6\text{ eV}$ for silicene. An asymmetric contribution of Σ_s on the valence and conduction bands is shown.

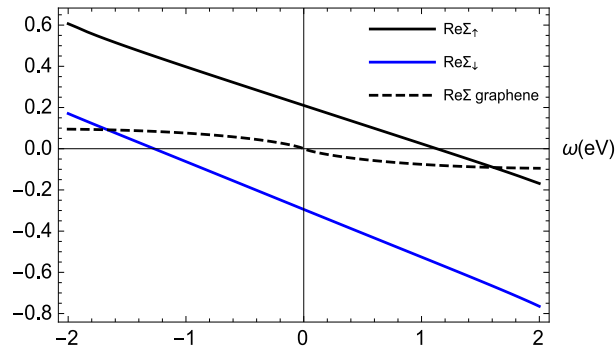


Figure 4: Polarized real part $\Re\Sigma_s$ of Σ_s in silicene compared with $\Re\Sigma$ in graphene near the Dirac point and vanishing electric field, and where $D = 7\text{eV}$, $V = 0.9\text{ eV}$, $\epsilon_0 = 0.2\text{ eV}$, $U = 0$ and $\lambda = 0.039\text{ eV}$. At the Dirac point, the quasiparticle residue in silicene with $E_z = 0$ is not zero.

3 Results and discussions

The spin-polarized occupation numbers can be computed using ρ_s of eq.(11) as

$$n_s = \int_{-D}^{\mu} \rho_s(\omega) d\omega \quad (14)$$

where μ is the Fermi level. In order to obtain unequal spin occupation numbers at the impurity $n_{\uparrow} \neq n_{\downarrow}$, we must determine eq.(11), where the polarized density of states ρ_s depend on n_{-s} . The computation of n_{\uparrow} and n_{\downarrow} implies solving a self-consistent equation for n_s as a function of μ . The Fermi energy can be tuned experimentally by applying an external voltage to the sample that adds or subtracts charge carriers, in the form of electrons or holes ([51], [52]). Before computing the self-consistency equations

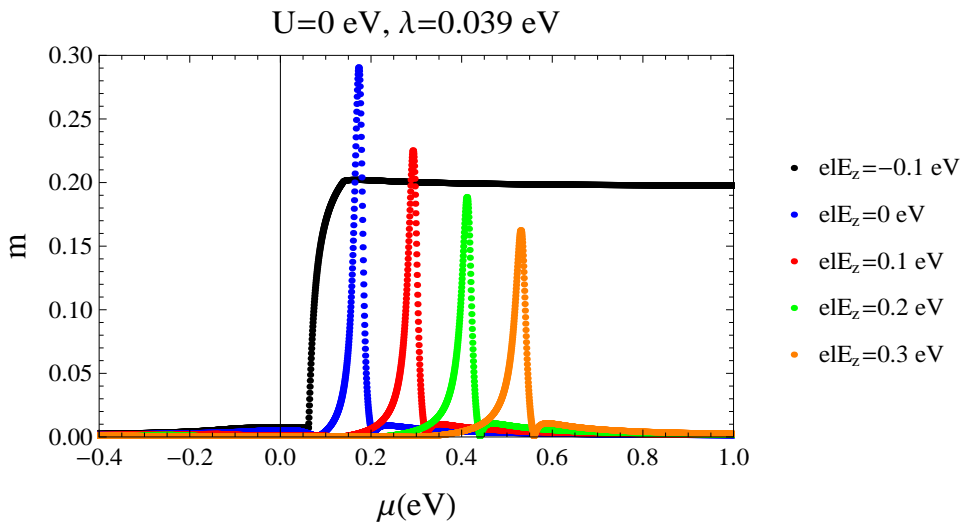


Figure 5: Local magnetic moment (in units of μ_B) as a function of μ for different values of elE_z in the $U = 0$ limit and where $V = 1$ eV and $\epsilon_0 = 0.2$ eV.

for the occupation numbers, we can study the limits $U = 0$ and $U \rightarrow \infty$. In the limit $U = 0$, local magnetism is possible due to the shift between polarized local density of states in the impurity created by λ_{so} . Because $U = 0$, the occupation numbers n_{-s} do not appear inside ρ_s and eq.(14) can be integrated without difficulty. In figure 5, the local magnetic moment in units of μ_B , where μ_B is the Bohr magneton, for $U = 0$ is shown as a function of μ for different values of elE_z where the peaks for $elE_z > 0$ correspond to the shift of the polarized density of states due to external electric field. On the other side, in the limit $U = \infty$, one of the quantities n_{\uparrow} or n_{\downarrow} is zero because, in the case $n_{\uparrow} \neq 0$, by putting a spin-down electron on the adatom implies infinite energy. Then, we can write without loss of generality that $n_{\downarrow} = 0$, then the local magnetic moment can be computed as $m = n_{\uparrow}(U = \infty)$ (see figure 6), where the local magnetic moment is shown as a function of μ for different values of elE_z and tends to $m = 1$ for large elE_z and vanishes for $E_z = 0$.

In order to describe local magnetism between these two limits, the self-consistent equations for n_s must be computed by starting with random values of n_{\uparrow} and n_{\downarrow} and computing $\rho_s(\omega)$ from eq.(11). This local density of states at the impurity is used through eq.(11) to obtain new values of n_{\uparrow} and n_{\downarrow} which are reintroduced in ρ_s . The iteration is done until the occupation numbers satisfy the condition $|n_s(i+1) - n_s(i)| < 10^{-6}$. In figures 7 (for $\epsilon_0 = 0.2$ eV) and 8 (for $\epsilon_0 = -0.2$ eV) the magnetic regime of the impurity atom as a function of $x = \pi V^2/UD$ and $y = (\mu - \epsilon_0 - (1+r)elE_z)/U$ is shown for different values of the electric field strength. In both figures we can compare the magnetic phases of the impurity atom in silicene, with and without electric field, with the magnetic phases in

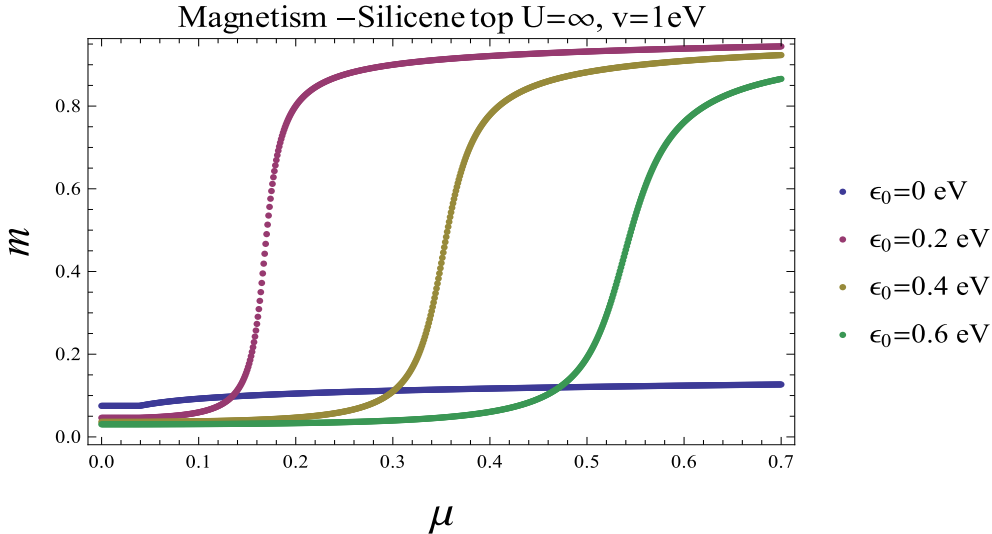


Figure 6: Local magnetic moment (in units of μ_B) as a function of μ for different values of ϵ_0 in the $U = \infty$ limit and where $V = 1$ eV and $E_z = 0$.

graphene, in terms of the Hamiltonian parameters $x = \frac{\pi V^2}{UD}$ and $y = \frac{\mu - \epsilon_0 - (1+r)elE_z}{U}$, where the local magnetic moment is given in units of μ_B (see the color bar in both figures). In both figures, for $x = 0$ there is a non-vanishing local magnetic moment for $\epsilon_0 < \mu < \epsilon_0 + U$ without electric field and for $\epsilon_0 + (1+r)elE_z < \mu < \epsilon_0 + U + (1+r)elE_z$. This is expected because the electric field only introduces a shift in the local energy of the impurity. As in graphene, the boundary in silicene is not symmetrical at $y = \frac{1}{2}$ and exhibits no particle-hole symmetry around $\mu = \epsilon_0 + (1+r)elE_z$ (see [53]) even for a top site adatom, where the orbital symmetry is irrelevant and the C_{3v} point group symmetry of the honeycomb sublattice is preserved by the adatom in the top site. Without electric field, there is a non-vanishing local magnetic moment when the Fermi level is below ϵ_0 for $\epsilon_0 > 0$ as it is shown in figure (7), which is a similar effect that than found in [42] for hollow site adsorption in silicene. In turn, the spin-orbit interaction stretches the boundary between phases towards the lower half plane and narrows it when the electric field is turned on.¹ The fact that the boundary between magnetic phases enlarges for silicene with $\lambda_{so} \neq 0$ and $E_z = 0$ implies that the suppression of the local broadening for $|\omega| < \lambda_{so}$ and the unequal spin shift factor $\Delta_s - \omega$ in eq.(12) allows the formation of spin moments for $\mu < \epsilon_0 - U$ and small U .

Due to the linear scaling of the broadening with ω of the impurity level, magnetism is allowed for Fermi energies $\mu > \epsilon_0 - \frac{3}{2}U$ well below the impurity energy ϵ_0 and this behavior is enhanced when the electric field is turned on. In figure 8, the same effect is shown for $\epsilon_0 = -0.2$ eV, where magnetism can be found when the Fermi level is larger than $\epsilon_0 + U$ and the boundary between magnetic phases shrinks in the y direction when the electric field is negative. By increasing the electric field strength, an asymmetric broadening of the impurity energy level is lifted by the modification of the imaginary part of the self-energy and in turn a shift in the impurity peak appears due to effective impurity energy $\epsilon_0 + (1+r)elE_z$.

In figure (9), the local magnetic moment is shown for different values of μ as a function of elE_z , where we have considered $V = 1$ eV, $\epsilon_0 = -0.2$ eV, $\lambda = 0.039$ eV and $U = 0.1$ eV. In both figures it can be seen that magnetism follows a linear relation between μ and E_z , caused by the shift in the density of states due to the effective impurity $\epsilon_0 + (1+r)elE_z$. When $\epsilon_0 + (1+r)elE_z + Un_{-s} < \mu < Un_s$, the occupation numbers are not identical. The boundary of the magnetic phases in this case is controlled

¹The electric field values used are smaller than the critical electric field at which the honeycomb structure of silicene becomes unstable $elE_z \sim 0.59$ eV (see [18]).

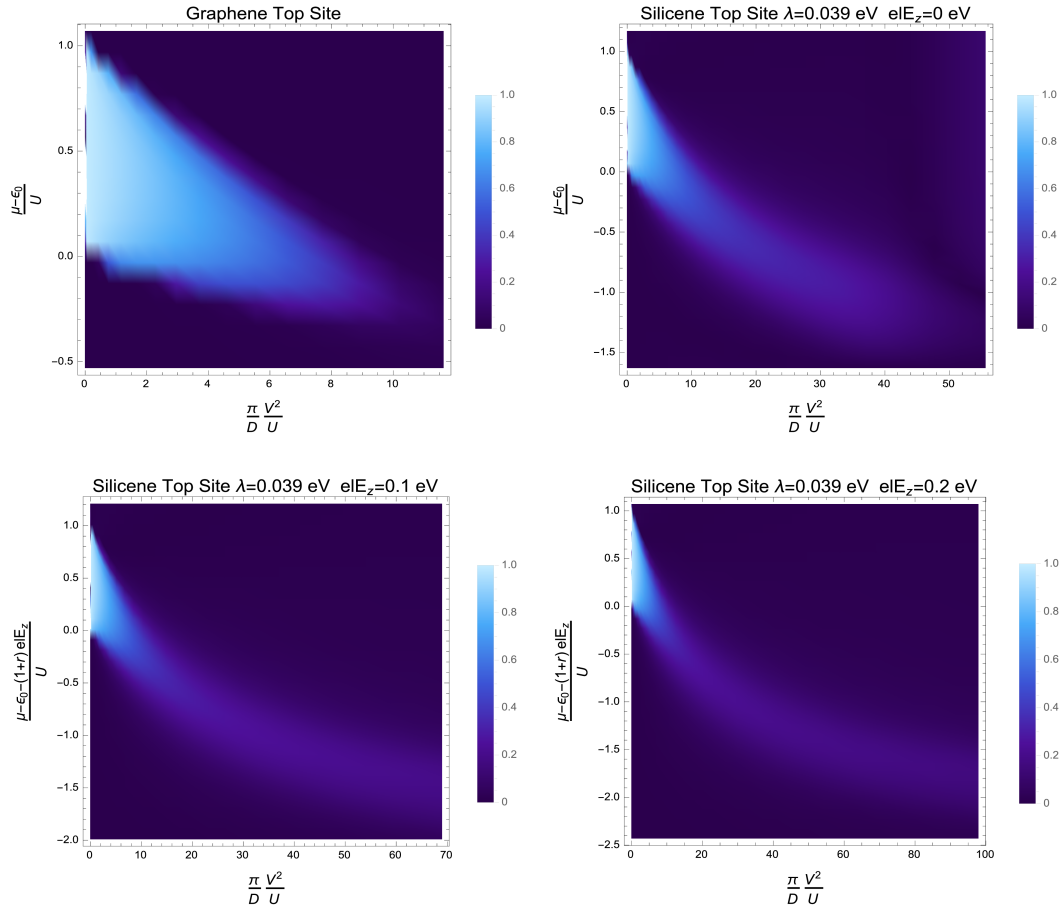


Figure 7: Local magnetic moment (in units of μ_B) in the impurity atom in the variables $x = \frac{\pi V^2}{UD}$ and $y = (\mu - \epsilon_0)/U$ for graphene and silicene with $E_z = 0$ and $x = \frac{\pi V^2}{UD}$ and $y = (\mu - \epsilon_0 - (1+r)elE_z)/U$, where $\epsilon_0 = 0.2$ eV which is above the Dirac point. The color bar indicates local magnetic moment in units of μ_B .

by the broadening of the peak. For $-0.85\text{eV} < elE_z < 0.35\text{eV}$ there is a local magnetic moment for $\mu > -0.4$ eV. When the impurity peaks in the polarized density of states of the impurity enters the gap zone, given by $-|\Delta_s| < \omega < |\Delta_s|$, and when $\mu > -|\Delta_s|$, the non-vanishing local magnetic moment is frozen for larger μ . Thus by manipulating the Fermi level with the applied gate voltage, an adatom interacting with silicene fulfills the requirement for the formation of a magnetic state due to the spin-asymmetric anomalous broadening and spin-asymmetric broadening gap for energies near the Dirac point. In turn, even for small U values [54] and Fermi energies below the effective on-site impurity energy, magnetism arises in the impurity carried by the itinerant electrons in the host lattice in contrast with transition metals adatoms, where it is harder to enhance the local magnetic moment for large U [55]. For low impurity concentrations, when the local magnetic moments are driven to an excited state, for example with an external electric field, dynamical spin-excitations are formed and are carried for long distances [56] which can be utilized in spintronic devices to develop magnetic information storage with electric gates [57]. Currently, X-ray magnetic circular dichroism (XMCD) and inelastic scanning tunneling spectroscopy are used to identify adatoms with magnetocrystalline anisotropy energy of few meV deposited on Graphene/SiC showing a paramagnetic behavior, with a magnetic moment out-of-plane for Co and Fe adatoms [58].

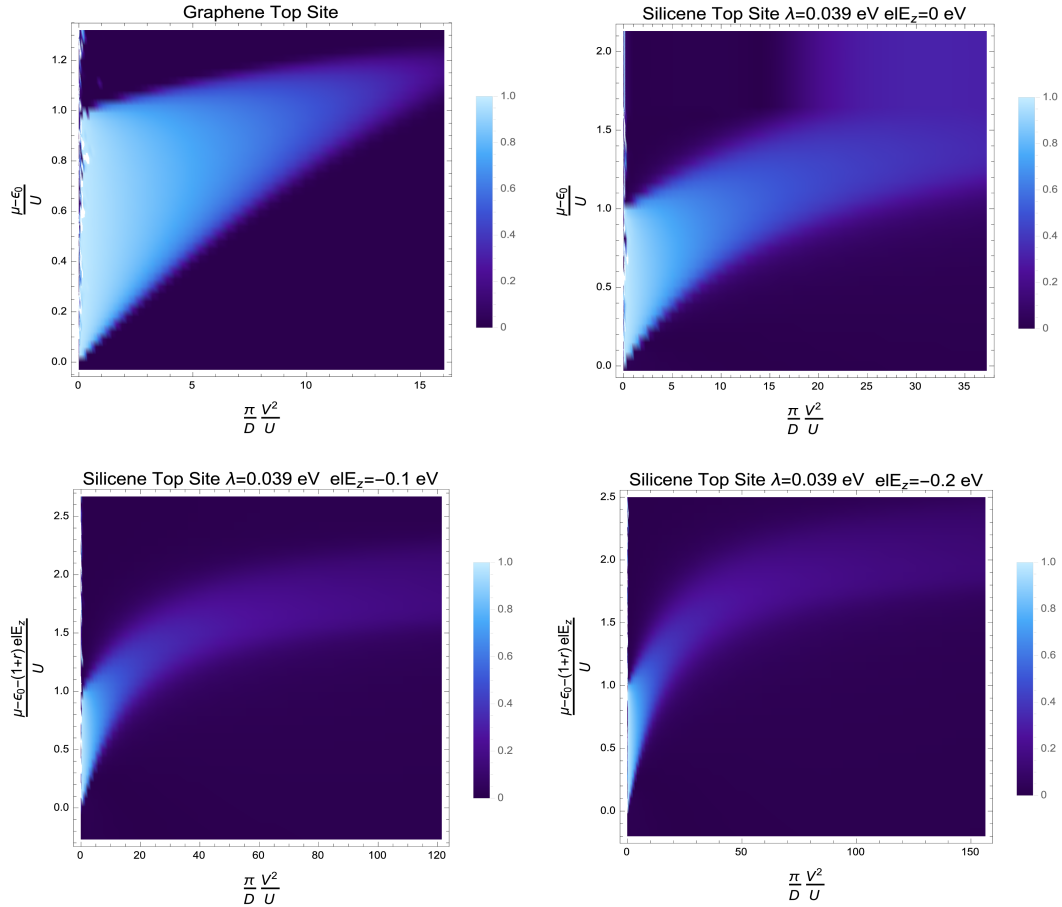


Figure 8: Local magnetic moment (in units of μ_B) in the impurity atom in the variables $x = \frac{\pi V^2}{UD}$ and $y = (\mu - \epsilon_0)/U$ graphene and silicene with $E_z = 0$ and $x = \frac{\pi V^2}{UD}$ and $y = (\mu - \epsilon_0 - (1+r)elE_z)/U$, where $\epsilon_0 = -0.2$ eV, which is below the Dirac point.

4 Conclusions

In this work we have studied the effect of the electric field on the formation of a local magnetic moment in an impurity adsorbed on a top site in silicene. By computing the polarized density of states in the impurity and solving the self-consistent equations for the occupation numbers in the mean-field approximation, we obtain the boundary of the magnetic phases for silicene with spin-orbit coupling and different electric field strengths, considering on-site impurity energies below and above the Dirac point. A local magnetic moment is formed for Fermi energies below the on-site impurity energy due to the broadening of the impurity level that scales linearly in $|\omega|$ with a shift due to the spin-orbit coupling and the external electric field. In turn, a gap in the broadening for $|\omega| < elE_z - s\lambda_{so}$ allows the local magnetic moment to be freezed when μ crosses the gap zone, even when $E_z = 0$. By increasing the electric field strength the boundary between magnetic phases stretches allowing a moment formation in silicene more easily than in graphene. The results obtained can be important to design spintronic devices, where the local magnetic moment can be controlled by an electric field application and to manipulate spin waves by considering different adatoms coverages of silicene subject to external oscillating electric fields.

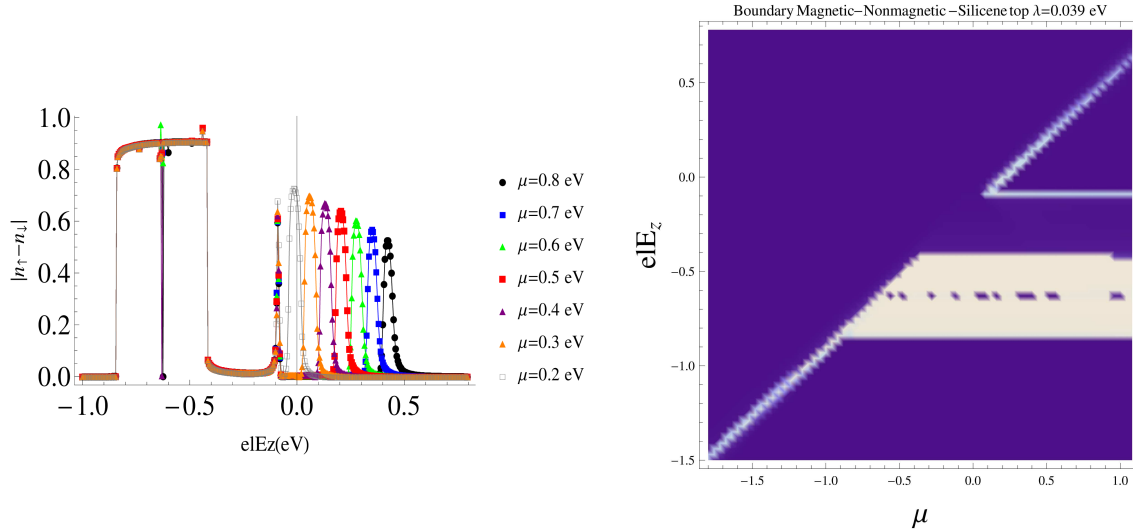


Figure 9: Left. Local magnetic moment $|n_{\uparrow} - n_{\downarrow}|$ (in units of μ_B) as a function of elE_z for different values of μ where $V = 1\text{eV}$, $U = 0.1\text{eV}$, $\lambda = 0.039\text{eV}$, $r = 0.3$ and $\epsilon_0 = -0.2$ eV. Right. Boundary between magnetic and non-magnetic zone in a μ - elE_z space for the same set of parameters V , U , λ , r and ϵ_0 . The straight line of local magnetism corresponds to the shifted peaks in the left figure.

5 Acknowledgment

This paper was partially supported by grants of CONICET (Argentina National Research Council) and Universidad Nacional del Sur (UNS) and by ANPCyT through PICT 1770, and PIP-CONICET Nos. 114-200901-00272 and 114-200901-00068 research grants, as well as by SGCyT-UNS., J. S. A. and P. J. are members of CONICET., F. E and J. V. are fellow researchers at this institution.

6 Author contributions

All authors contributed equally to all aspects of this work.

References

- [1] G. G. Guzmán-Verri and L. C. L. Y. Voon, *Phys. Rev. B* **76**, 075131 (2007).
- [2] M. Houssa, A. Dimoulas, A. Molle, *Jour. Phys. Cond. Matt.*, **27** (25), 253002 (2015).
- [3] A. Geim, *Science* **324**, 1530 (2009).
- [4] C. V. Nguyen, N. N. Hieu, *Chem. Phys.*, **468**, 9 (2016).
- [5] M. J. Spencer, T. Morishita (Eds.), *Silicene*, Springer International Publishing, 2016.
- [6] N. Gillgren, D. Wickramaratne, Y. Shi, T. Espiritu, J. Yang, J. Hu, J. Wei, X. Liu, Z. Mao, K. Watanabe, T. Taniguchi, M. Bockrath, Y. Barlas, R. K. Lake, C. Ning Lau, *2D Mater.*, **2** 011001 (2014).
- [7] E. Bianco, S. Butler, S. Jiang, O. D. Restrepo, W. Windl, J. E. Goldberger, *ACS Nano* **7**, 4413 (2013).

- [8] P. T. T. Le, M. Yarmohammadi, *Chem. Phys.*, **519**, 1-5 (2019).
- [9] R. Roldán, L. Chirulli, E. Prada, J. A. Silva-Guillén, P. San Jose and F. Guinea, *Chem. Soc. Rev.*, **15** (2017).
- [10] M. Yarmohammadi, *Phys. Rev. B*, **98**, 155424 (2018).
- [11] P. De Padova, C. Quaresima, C. Ottaviani, P. M. Sheverdyeva, P. Moras, C. Carbone, D. Topwal, B. Olivieri, A. Kara, H. Oughaddou, B. Aufray, and G. Le Lay, *Appl. Phys. Lett.*, **96**, 261905 (2010).
- [12] P. Vogt, P. De Padova, C. Quaresima, J. Avila, E. Frantzeskakis, M. C. Asensio, A. Resta, B. Ealet, and G. Le Lay, *Phys. Rev. Lett.*, **108**, 155501 (2012).
- [13] A. Fleurence, R. Friedlein, T. Ozaki, H. Kawai, Y. Wang, and Y. Yamada-Takamura, *Phys. Rev. Lett.*, **108**, 245501 (2012).
- [14] M. Houssa, E. Scalise, K. Sankaran, G. Pourtois, V. V. Afanas'ev, A. Stesmans, *Appl. Phys. Lett.*, **98** (22), 223107 (2011).
- [15] R. Winkler and U. Zülicke, *Phys. Rev. B*, **82**, 245313 (2010).
- [16] N. Y. Dzade, K. O. Obodo, S. K. Adjokatse, A. C. Ashu, E. Amankwah, C. D. Atiso, A. A. Bello, E. Igumbor, S. B. Nzabarinda, J. T. Obodo, A. O. Ogbuu, O. E. Femi, J. O. Udeigwe, U. V. Waghmare, *J. Phys.: Condens. Matter*, **22** (37), 375502 (2010).
- [17] S. Lebegue and O. Eriksson, *Phys. Rev. B*, **79**, 115409 (2009).
- [18] N. D. Drummond, V. Zlyomi, V. I. Fal'ko, *Phys. Rev. B*, **85** (7), 3702 (2012).
- [19] Z. Ni, Q. Liu, K. Tang, J. Zheng, J. Zhou, R. Qin, Z. Gao, D. Yu, J. Lu, *Nano Letters*, **12** (1), 113–118 (2012).
- [20] C. C. Liu, H. Jiang, Y. Yao, *Phys. Rev. B*, **84** (19), 195430 (2011).
- [21] Y. Yao, F. Ye, X. L. Qi, S. C. Zhang, Z. Fang, *Phys. Rev. B*, **75** (4) 041401 (2007).
- [22] C. C. Liu, W. Feng, Y. Yao, *Phys. Rev. Lett.*, **107** (7), 076802 (2011).
- [23] M. Ezawa, *Phys. Rev. B*, **87** (15) 155415 (2013).
- [24] M. Yarmohammadi and K. Mirabbaszadeh, *Commun. Theor. Phys.*, **67**, 5 (2017).
- [25] E. Rotenberg, *Graphene Nanoelectronics*, in: H.Raza (Ed.), Springer-Verlag, Berlin, Heidelberg, 2012.
- [26] F. Escudero, J. S. Ardenghi, L. Sourrouille, P. Jasen and A. Juan, *Super. and Micro.*, **113**, 291-300 (2018).
- [27] J. S. Ardenghi, P. Bechthold, E. Gonzalez, P. Jasen, A. Juan, *Super. and Micro.*, **72**, 325-335, (2014).
- [28] J. S. Ardenghi, P. Bechthold, E. Gonzalez, P. Jasen, A., *Eur. Phys. J. B*, **88**: 47 (2015).
- [29] J. S. Ardenghi, P. Bechthold, P. Jasen, E. Gonzalez, O. Nagel, *Physica B*, **427**, 97-105, (2013).
- [30] Y. V. Skrypnik and V. M. Loktev, *Phys. Rev. B* **73**, 241402(R) (2006).
- [31] J. O. Sofo, G. Usaj, P. S. Cornaglia, A. M. Suarez, A. D. Hernandez-Nieves, and C. A. Balseiro, *Phys. Rev. B* **85**, 115405 (2012).

- [32] A. C. Hewson, *The Kondo problem to heavy fermions* (Cambridge University Press, Cambridge, 1997).
- [33] J. Ren, H. Guo, J. Pan, Y. Y. Zhang, X. Wu, H.-G. Luo, S. Du, S. T. Pantelides, and H.-J. Gao, *Nano Lett.* **14**, 4011 (2014).
- [34] B. Aufray, A. Kara, S. Vizzini, H. Oughaddou, C. Léandri, B. Ealet and G. Le Lay, *Appl. Phys. Lett.* **96** 183102 (2010).
- [35] E. Cinquanta, E. Scalise, D. Chiappe, C. Grazianetti, B. van den Broek, M. Houssa, M. Fanciulli and A. Molle, *J. Phys. Chem. C*, **117** 16719–24 (2013).
- [36] N. Y. Dzade, K. O. Obodo, S. K. Adjokatse, A. C. Ashu, E. Amankwah, C. D. Atiso, A. A. Bello, E. Igumbor, S. B. Nzabarinda, J. T. Obodo, A. O. Ogbuu, O. E. Femi, J. O. Udeigwe and U. V. Waghmare, *J. Phys.: Condens. Matter*, **22** 375502 (2010).
- [37] V. Q. Bui, T. T. Pham, H. V. S. Nguyen and H. Le, *J. Phys. Chem. C*, **117** 23364–71 (2013).
- [38] Y. Liu, X. Zhou, M. Zhou, M.-Q. Long, G. Zhou, *J. Appl. Phys.*, **116** (24) 244312 (2014).
- [39] F. Escudero, J. S. Ardenghi and P. Jasen, *Jour. Magn. Magn. Mat.*, **454**, 131-138 (2018).
- [40] F. Escudero, J. S. Ardenghi and P. Jasen, *J. Phys. Condens. Matter*, **30**, 275803 (2018).
- [41] P. W. Anderson, *Phys. Rev.*, **124**, 41 (1964).
- [42] J. Villarreal, J. S. Ardenghi and P. Jasen, *Superlattice. Microst.*, **130** (285-296) 2019.
- [43] M. Laubach, J. Reuther, R. Thomale, S. Rachel, *Phys. Rev. B* **90**, 165136 (2014).
- [44] C. L. Kane and E. J. Mele, *Phys. Rev. Lett.*, **95**, 226801 (2005).
- [45] M. Zare, *Phys. Rev. B*, **100**, 085434 (2019).
- [46] H. M. Le, T. T. Pham, T. S. Dinh, Y. Kawazoe, and D. Nguyen-Manh, *J. Phys.: Condens. Matter*, **28**(13), 135301 (2016).
- [47] S. Nigam, S. K. Gupta, C. Majumder and R. Pandey, *Phys. Chem. Chem. Phys.*, **17**, 11324 (2015).
- [48] B. Uchoa, L. Yang, S. W. Tsai, N. M. R. Peres, and A. H. Castro Neto, *Phys. Rev. Lett.* **103**, 206804 (2009).
- [49] B. Uchoa, L. Yang, S.-W. Tsai, N. M. R. Peres, A. H. Castro Neto, *New Journal of Physics* **16**, 013045 (2014).
- [50] M. A. Romero, A. Iglesias-Garcia and E. C. Goldberg, *Phys. Rev. B*, **83** 125411 (2011).
- [51] R. R. Nair, I.-L. Tsai, M. Sepioni, O. Lehtinen, J. Keinonen, A. V. Krasheninnikov, A. H. Castro Neto, M. I. Katsnelson, A. K. Geim, and I. V. Grigorieva, *Nat. Commun.* **4**, 2010 (2013).
- [52] N. A. Pike and D. Stroud, *Phys. Rev. B*, **89** 115428 (2014).
- [53] B. Uchoa, V. N. Kotov, N. M. R. Peres, and A. H. Castro Neto, *Phys. Rev. Lett.* **101**, 026805 (2008).
- [54] S. K. Pati, T. Enoki and C. N. R. Rao, *Graphene and its fascinating attributes*, World Scientific Publishing, 2011 (chapter 7).
- [55] M. Manadé, F. Viñes, and F. Illas, *Carbon*, **95**:525 (2015).

- [56] F. S. M. Guimaraes, D. F. Kirwan, A. T. Costa, R. B. Muniz, D. L. Mills, and M. S. Ferreira, *Phys. Rev. B* **81**, 153408 (2010).
- [57] Li Tao, E. Cinquanta, D. Chiappe, C. Grazianetti, M. Fanciulli, M. Dubey, A. Molle and D. Akinwande, *Nature Nanotech.* **10**, 227–231 (2015)
- [58] T. Eelbo, M. Wasniowska, P. Thakur, M. Gyamfi, B. Sachs, T. O. Wehling, S. Forti, U. Starke, C. Tieg, A. I. Lichtenstein, and R. Wiesendanger, *Phys. Rev. Lett.* **110**, 136804 (2013).